2021

Numerical and Experimental Steady-State Investigation of Supercritical CO2 Gas Cooler Plate Heat Exchanger

Saad Jalil
Michigan State University

Ahmed Okasha
Michigan State University, aokasha@msu.edu

James Gebbie
Ford Motor Company

Norbert Müller
Michigan State University

Numerical and Experimental Steady State Investigation of Supercritical CO_2 Gas Cooler Plate Heat Exchanger

S. M. Jalil [1,2*], Ahmed Okasha [1], James G. Gebbie [3], Norbert Müller [1]
[1] Department of Mechanical Engineering, Michigan State University, East Lansing, MI, USA
[2] Department of Mechanical Engineering, University of Anbar, Ramadi, Anbar 31001, Iraq
[3] Ford Motor Company, Dearborn, MI, USA

saad.jalil@uoanbar.edu.iq | aokasha@msu.edu | jgebbie@ford.com | mueller@egr.msu.edu

* Corresponding Author

ABSTRACT

Natural environmentally friendly refrigerants have been considered as alternatives to HFC refrigerants with high Global Warming Potential. In transcritical R744 vapor compression cycles, the heat rejection process occurs above the critical point where the temperature and the pressure are independent of each other. In this work, the gas cooling in a commercial 20 plate heat exchanger (PHE) used as gas cooler is modeled numerically and compared to experimental results. The numerical model is a simplified 2D model, i.e. corrugated plates with zero chevron angle. Four different real gas models are tested in terms of agreement and convergence, and numerical results from four cases with CO_2 pressure ranging from 80 to 95 bar are compared with experimental results. Each case is numerically modeled with surface area that is set to match total surface area of the 20 PHE, and with one and half times the surface area of the 20 PHE. The increase in the surface area is shown to compensate for the chevron angle effect. For the experimental investigation, a CO_2 heat pump test rig is used that supports cooling and heating applications. The numerical results show that the PHE outlet temperatures are in good agreement with the experimental results. The simplified 2D numerical models could reduce the computational costs associated with 3D PHE numerical simulations.

1. INTRODUCTION

Under Kyoto protocol regulations (adopted in 1997 and entered into force in 2005), the phase out of HFC refrigerants is underway due to their high GWP. The US EPA has listed R134a as unacceptable for newly manufactured light-duty vehicles beginning in Model Year 2021 (Chakrabarti, *et al.*, 2017). For more than a decade, carbon dioxide (CO_2, R744) has been revived as a natural environmentally friendly refrigerant. Compared to HFC refrigerants with a GWP in the order of 1300-1900, R744 has a GWP of one. Several CO_2 transcritical cycle analyses contributing to the understanding have been carried out by (Kim *et al.*, 2004), (Nekså, 2004), (Müller and Joseph, 2009), and (Lorentzen, 1994). CO_2 distinguishes itself from common refrigerants by its relatively low critical temperature and high critical pressure of 31.1 °C and 73.8 bar, respectively. For a transcritical heat pump cycle that operates at high ambient/sink temperatures and can be used for either cooling or heating applications, the heat rejection process at the high-pressure side takes place above the critical point. While in the subcritical two-phase region, pressure and temperature are coupled by the saturation curve; in the supercritical region, pressure and temperature are independent of each other. Therefore, in the supercritical region, for a given ambient temperature that can be related to the gas cooler (GC) outlet temperature (Kauf, 1999), the GC pressure (high-side pressure) can be controlled independently and utilized for cycle optimization.

Several manufacturers supply plate heat exchangers that are compatible with CO_2. They are compact in design and support liquid CO_2 applications. Galeazzo *et al.* (2006) have studied experimentally and numerically the heat transfer in a plate heat exchanger with two flow arrangements. Their 3D numerical model has been carried out for four flat plates without corrugations as a virtual prototype. They have shown that the series flow arrangement is in better agreement with the experimental data compared to the parallel flow arrangement. Han *et al.* (2010) have carried out a 3D numerical simulations and experimental investigation to study the flow field pattern in corrugated plate heat exchanger. They have studied a five-plate heat exchanger and have shown the temperature, pressure, and velocity fields distributions. They have indicated that the PHE performance is affected by the non-uniform distribution of the

fluid flow. Jain *et al.* (2007) have used chevron-corrugated plates to study the heat transfer and flow fields inside a four-plate heat exchanger. They have presented the underpredicted percentage in the fraction factor and Nusselt number in their 3D numerical simulations and experimental results compared with previous empirical correlations. (Skočilas and Palaziuk, 2015) have numerically studied the heat transfer enhancement in a two-plate heat exchanger. They have shown from their 3D simulations that the heat transfer coefficient is enhanced with chevron plates compared to flat plates. Further, they have shown that increasing the chevron angle increases the pressure drop. (Han, et al., 2011) have studied the heat transfer from double-sinusoidal corrugated plates using water as a working fluid. The have shown that the deviation between their 3D numerical simulation results and literature experiments are within $\pm$20%. They have used the approximation-assisted optimization to study the optimum design for the PHE. They also have shown that the angle of corrugation is considered one of the important factors that affect the PHE design.

In the work discussed here, a numerical model is developed for a commercial plate heat exchanger acting as a gas cooler in a transcritical CO_2 heat pump system. To reduce complexity and time for the computational simulation, the plates with sinusoidal corrugation are modeled in 2D instead of modeling them in 3D. This means the chevron angle effect is eliminated. To compensate for the chevron angle effect, the total surface area of the plate heat exchanger is increased, and the effect is explored with numerical simulations. Four experimental test cases are conducted at CO_2 inlet pressures of 80, 85, 90, and 95 bar, utilizing a newly built CO_2 heat pump test rig that supports cooling and heating applications. The results of the CO_2 and secondary heat transfer fluid (HTF) outlet temperatures are compared with the numerical simulations. Also, the performance of four real gas models is tested in the numerical simulations.

2. NUMERICAL MODELING

2.1. Governing equations and numerical approach

The continuity, momentum, and energy equations for the current study are solved by using the transient SIMPLE scheme of the pressure-velocity coupling method in FLUENT 19.1 (ANSYS, 2016) (Patankar, 1980). The two-equations pressure-based realizable k-ε turbulent model is used for modeling the Reynolds stresses term ($-\rho\overline{u_i' u_j'}$) with enhanced wall function. k and ε are the turbulence kinetic energy (m^2/s^2) and its dissipation rate (m^2/s^3). The instantaneous velocity (u_i) consists of the mean component ($\overline{u_i}$) and the fluctuating component (u_i'). This turbulent model is employed in the simulations to solve the Reynolds-Averaged Navier-Stokes (RANS) equations as (ANSYS, 2016) (Jalil S. , 2019)

$$\frac{\partial \rho}{\partial t} + \frac{\partial (\rho \overline{u_i})}{\partial x_i} = 0 \tag{1}$$

$$\frac{\partial (\rho \overline{u_i})}{\partial t} + \frac{\partial (\rho \overline{u_i u_j})}{\partial x_j} = -\frac{\partial \overline{p}}{\partial x_i} + \frac{\partial}{\partial x_j}\left[\mu\left(\frac{\partial \overline{u_i}}{\partial x_j} + \frac{\partial \overline{u_j}}{\partial x_i}\right)\right] + \frac{\partial}{\partial x_j}(-\rho\overline{u_i' u_j'}) \tag{2}$$

Depending on the conjugate heat transfer between the fluids and the walls of the PHE, the energy equation is solved with the existence of a coupling wall or an interface between the fluids and solids as shown in Eqn. (3) (Jalil S., 2020) with ignoring the external source and the viscous heat dissipation term.

$$\frac{\partial (\rho c_p T)}{\partial t} + \frac{\partial (\rho c_p \overline{u_i} T)}{\partial x_j} = \frac{\partial}{\partial x_j}\left[k\frac{\partial T}{\partial x_j} - \rho c_p \overline{u_i' T'}\right] \tag{3}$$

The convergence criteria is set for the normalized residual in the order of $1 * 10^{-9}$ for the energy equation and $1 * 10^{-6}$ for all other governing equations with 5000 iterations to ensure their convergence to the specified residual limit. In addition, a time step size of $1 * 10^{-6}$ second is considered to achieve a stable solution. The Redlich–Kwong real gas model is selected to represent the cubic equation of state and calculate the density of CO_2 (ANSYS, 2016)

$$p = \frac{RT}{V - b} - \frac{\alpha_o}{(T/T_c)^{0.5}(V^2 + bV)} \tag{4}$$

where α_o and b are constants related to the fluid critical pressure and temperature

$$\alpha_o = \frac{0.42747 R^2 T_c^2}{p_c} \quad , \quad b = \frac{0.08664 R T_c}{p_c} \tag{5}$$

Beside the Redlich-Kwong model, also the Aungier- Redlich-Kwong, Peng-Robinson, and Soave- Redlich-Kwong real gas models are tested under the initial and boundary conditions that are listed in Table 1. For all cases, maintaining the same mass flow rate is achieved by trial and error matching the experimental values for CO_2 and HTF within 4% as shown in Table 1. The computations show the Redlich–Kwong model as the fastest with results very close to those of the other models. All models showed the same deviation in the outlet temperature of the CO_2, which is less than 15%. The deviation in the CO_2 gas cooling across the heat exchanger is calculated and compared with experimental temperature drop as defined in Eqn. (6). This deviation between the computational and experimental results is primarily related to the chevron angle, which is zero in the numerical study, because the study is in 2D. Table 1 shows the calculated input and output values for the experimental case with p=85 bar compared to the numerical simulation with the four real gas models tested. In all simulations, the CO_2 outlet temperature is higher and the HTF outlet temperature is lower than in the experimental results, because of the zero chevron angle in the study.

$$\text{Deviation} = \frac{\left(T_{CO2_{in}} - T_{CO2_{out}}\right)_{Exp} - \left(T_{CO2_{in}} - T_{CO2_{out}}\right)_{Num}}{\left(T_{CO2_{in}} - T_{CO2_{out}}\right)_{Exp}} * 100\% \tag{6}$$

Table 1: Numerical results obtained with four real gas models compared with experimental data at p=85 bar

Parameter	**Experimental**	**Numerical**			
		Redlich-Kwong	**Aungier- Redlich-Kwong**	**Peng-Robinson**	**Soave- Redlich-Kwong**
$\mathbf{p_{CO2_{in}}}$ (bar)	85.164	85	85	85	85
$\mathbf{p_{HTF_{in}}}$ (bar)	6	6	6	6	6
$\mathbf{m_{CO2_{in}}}$ (kg/s)	0.0201	0.0195	0.0195	0.0191	0.0194
$\mathbf{m_{HTF_{in}}}$ (kg/s)	0.0574	0.06	0.06	0.06	0.06
$\mathbf{T_{CO2_{in}}}$ (°C)	108.13	108	108	108	108
$\mathbf{T_{HTF_{in}}}$ (°C)	34.7	34.7	34.7	34.7	34.7
$\mathbf{T_{CO2_{out}}}$ (°C)	39.28	49.23	48.64	48.80	49.03
$\mathbf{T_{HTF_{out}}}$ (°C)	50.96	43.34	43.36	43.42	43.46
Deviation (%) in $\mathbf{T_{CO_2{}_{out}}}$		14.3	14.3	14.3	14.3

The HTF is water-ethylene-glycol mixture (50% - 50%) simulated with constant physical properties for each pressure case. The physical properties are calculated at the average between the inlet and outlet temperatures. Table 2 shows the calculated properties for the four pressure cases (80, 85, 90, and 95 bar) investigated experimentally and numerically.

2.2. Geometry and Mesh generation

Figure 1 shows a schematic for a 3D plate heat exchanger. The dimensions reflect the surface area of the plate heat exchanger used in the experiment. Figure 2 shows a section of the plate and each flow domain with its dimensions and the corrugated sine wave. The total length of the plate is 170 mm, which includes 32 sine waves (160 mm) plus 5 mm of a straight portion at the inlet and outlet of the modeled plate. The required surface area is achieved by setting the depth in the Fluent reference values dialog box to 666.7 mm. This depth provides a total heating surface area close to the experimental heating surface area of 0.24 m^2. For a unity depth of the 2D model, a depth of 1000 mm is used in the Fluent reference value dialog box to show the effect of increasing the surface area by a factor of 1.5. Increasing

the surface area is to substitute for the chevron angle effect and better match the numerical to the experimental results. The depth reference value used in Fluent is mentioned here, because most of the previous studies have considered a unity depth. Figure 2 also shows boundary conditions for the numerical simulations. The 2D domain is generated with structured uniform meshes of quadrilateral elements and refined meshes near the walls for both fluids to better resolve the flow in the boundary layer.

Table 2: Physical properties of water-ethylene-glycol mixture

p (bar)	T (°C)	μ (kg/m.s)	c_p (J/kg.K)	ρ (kg/m^3)	k (W/m.K)
85	42.85	0.0014	3514.3	1052.9	0.4174
95	41.72	0.0014	3510.3	1053.5	0.4167

Figure 1: 3D model for the 20 Plates heat exchanger

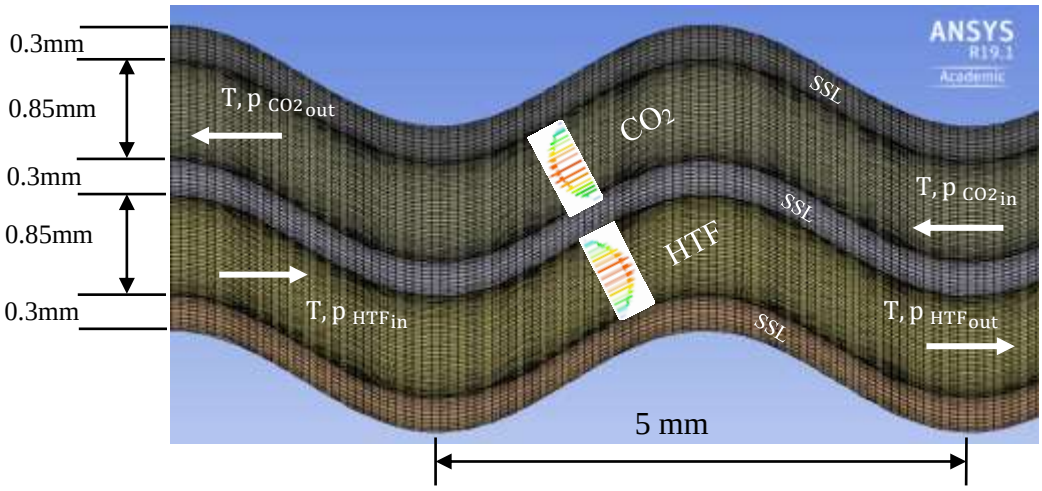

Figure 2: Numerical domains, dimensions and meshes for the studied plate heat exchanger

To achieve a grid-independent convergence, five meshes (mesh 1-5) are generated and tested under the same working conditions to inform the choice of a good mesh size. The mesh independent test indicates less than 0.001% change in the outlet temperature after mesh 1 (M1). Figure 3 shows the outlet temperatures and the mass flow rates for both the hot and cold fluid for the five generated meshes at p=85bar. Mesh 3 (M3) with 95270 cells is selected for all numerical simulations.

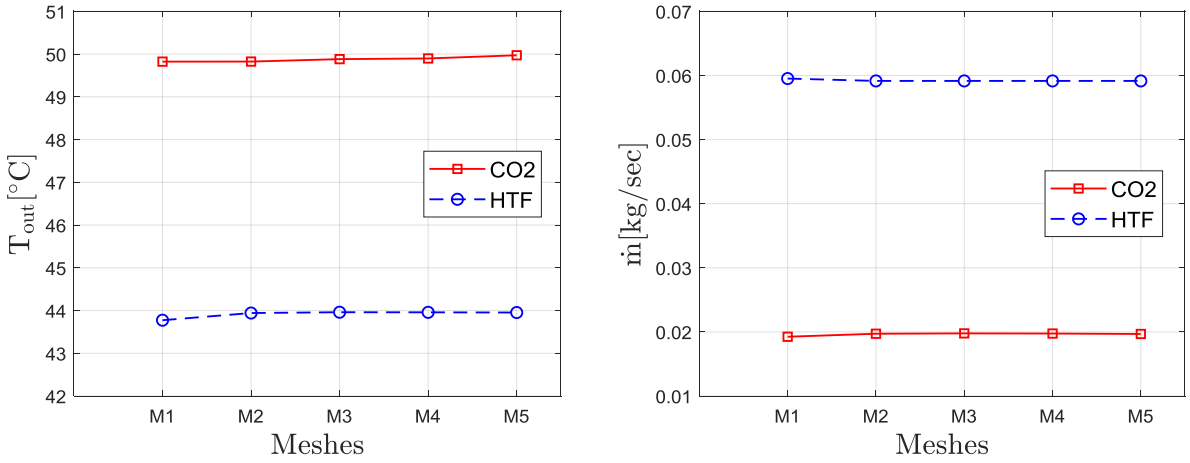

Figure 3: Outlet temperatures (left) and the mass flow rates (right) for both CO_2 (hot) and HTF (cold) at five mesh independent test cases (M1:25071, M2:47854, M3:83415, M4:125178, M5:224644)

Table 3 shows the input pressures, mass flow rates, and temperatures input for the four pressure cases (80, 85, 90, and 95 bar) investigated experimentally and numerically.

Table 3: Boundary conditions for the four cases

Parameter	**80 bar**	**85 bar**	**90 bar**	**95 bar**
$\mathbf{p_{CO2_{in}}}$ **(bar)**	80.208	85.164	90.215	94.863
$\mathbf{p_{HTF_{in}}}$ **(bar)**	6	6	6	6
$\mathbf{m_{CO2_{in}}}$ **(kg/s)**	0.0200	0.0201	0.0177	0.0146
$\mathbf{m_{HTF_{in}}}$ **(kg/s)**	0.0580	0.0574	0.0595	0.0604
$\mathbf{T_{CO2_{in}}}$ **(°C)**	96.99	108.13	118.42	134.94
$\mathbf{T_{HTF_{in}}}$ **(°C)**	35.13	34.74	33.64	33.19

3. EXPERIMENTAL PLANT & VALIDATION

The experimental test rig consists of a compressor, a gas cooler and an evaporator brazed plate heat exchanger, a manual expansion device, and an accumulator. The compressor is a commercial semi-hermetic single-stage, 1.34 kW, 3 phase, 230V, and 60 Hz. A manual metering valve is used as an expansion device that has a maximum pressure of 193 bar at 454 °C and a temperature range of -53 °C to 454 °C. An oil separator is installed at the compressor discharge with an oil sensor connected to a solenoid valve located at the return line to open/close according to the oil accumulation in the return line. The accumulator is an in-house design based on the estimated system volume. For compactness of the test-rig the accumulator is implemented horizontally. A chiller supplies both the gas cooler and the evaporator HTF loops with Water/Ethylene-Glycol mixture (50%-50% by volume). A 220 V immersion electric heater is placed before the inlet of each heat exchanger HTF line to independently control the inlet temperatures. The experimental test rig schematic and photographs are shown in Figure 4 and Figure 5, respectively.

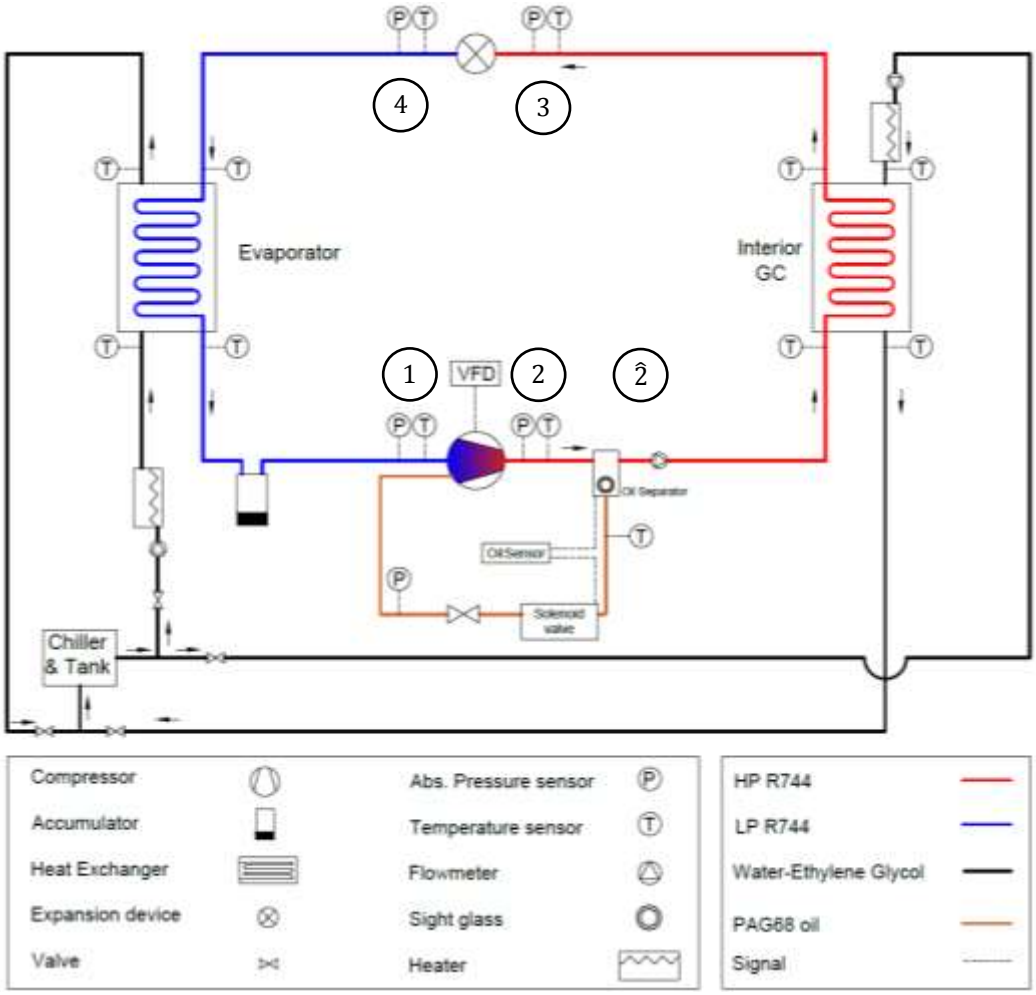

Figure 4: Experimental test rig layout

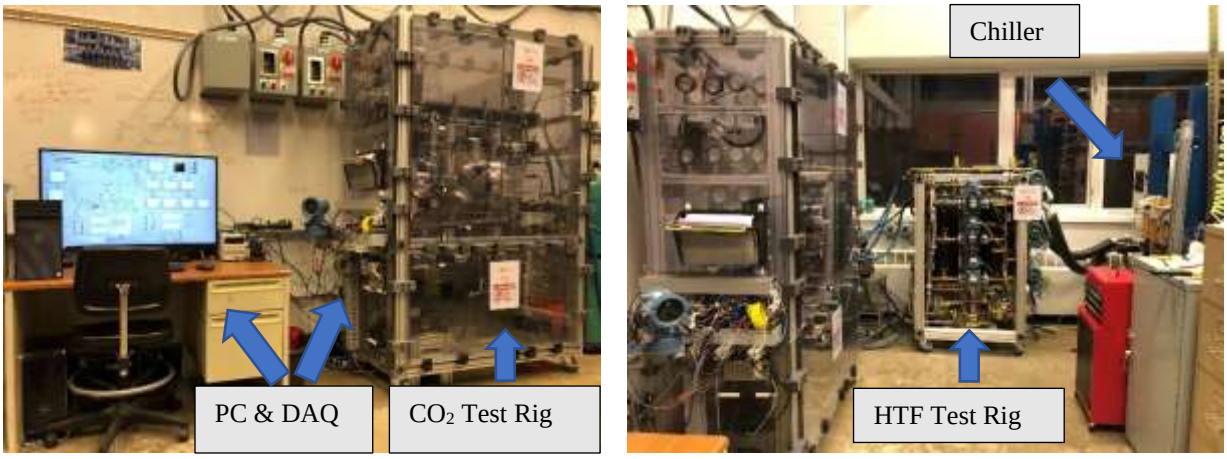

Figure 5: Front and side views of the experimental test rig. The front view shows the CO_2 test rig with the data acquisition and PC. The side view shows the HTF test rig connected to both the chiller and the CO_2 test rig from the right side and left side, respectively.

The steady state criteria for each test point is based on checking the energy balance (y) across the heating capacity, the cooling capacity, the compressor power, and the oil separator as shown in Equation (7). The oil separator is included in the equation because of the heat loss in the transient period that gradually decreases as the system approaches the steady state. The equation is normalized with respect to the HTF gas cooler capacity. The moving average is calculated for the variable y. In all the measurements, the moving average of the variable y is bounded within ±0.4%. For each measurement, when steady state is reached, the data is recorded for five minutes and the mean value of each measured variable is computed to represent the test point steady state measurement.

$$y\,(\%) = \frac{\dot{Q}_H + \dot{Q}_{OS} - \dot{Q}_C - \dot{W}_{comp}}{\dot{Q}_H} \tag{7}$$

4. RESULTS & DISCUSSION

Figure 6 and Figure 7 show the experimental CO_2 and HTF outlet temperature results vs. the numerical results at GC pressure of 80, 85, 90, and 95 bar. The numerical results follow the trend of the experimental results with different degree of agreement. As discussed before, the current study has not taken into consideration the chevron angle effect and it has alternatively replaced its effect by an increased surface area. Figure 7 presents the outlet temperature for CO_2 from the experiment and the simulation with same surface area and 1.5 surface area. The numerical results with 1.5 surface area are closer to the experimental results because of the increased rate of heat transfer between the CO_2 and the HTF. Figure 8 shows that the HTF temperatures from numerical simulation are less than the experimental temperatures, which means that the GC did not transfer as much energy from the hot CO_2 gas, not considering the thermal effect of the chevron angle presence. In practical PHE, chevron angles and corrugation play an essential role in enhancing the heat transfer performance of the gas cooler. As expected, increasing the surface area improves the heat transfer rate and the CO_2 cooling.

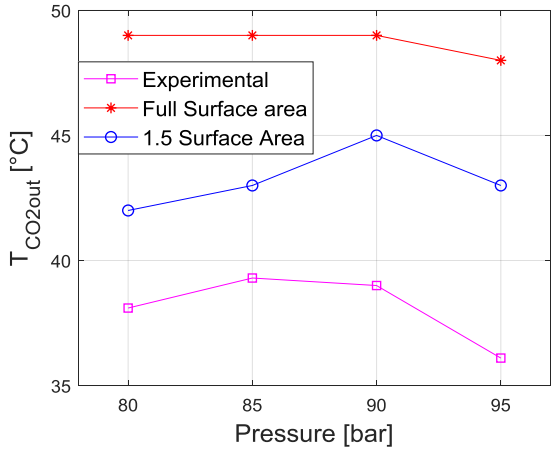

Figure 6: CO_2 gas cooler outlet temperature from numerical simulations with same and one and half surface area and from experiment

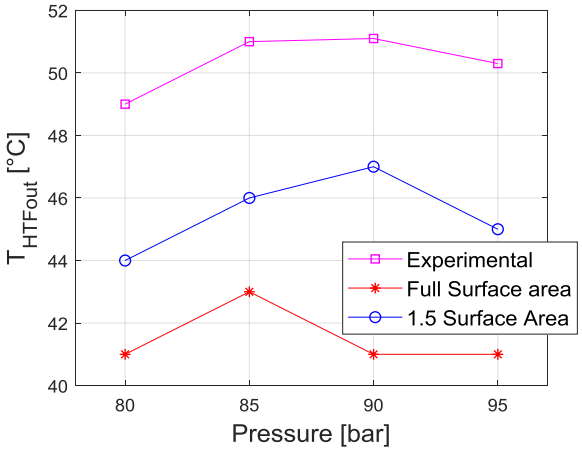

Figure 7: HTF gas cooler outlet temperature from numerical simulations with same and one and half surface area and from experiment

Figure 8 illustrates the corresponding deviation for CO_2 in Figure 6. The deviation between the numerical and experimental results calculated by Eqn. (6) reduces from 19 % to 7% in average.

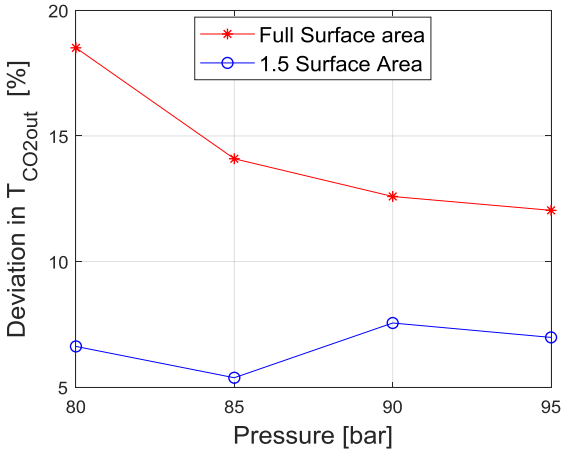

Figure 8: Deviation of the numerical gas cooler outlet temperatures from the experimental data for the results shown in Figure 6

Figure 9 and Figure 10 show the local Nusselt number along the cold and hot surfaces of the middle-corrugated plate for the full surface area cases. The local Nusselt number is calculated, monitored, and saved by Fluent using a built-in correlation (ANSYS, 2016), where the hydraulic diameter is the characteristic length for the internal flow. The ~30% fluctuation of the Nusselt number follows the plate corrugation with the moving average increasing from x=0 to x=170 mm, where the temperature difference at 85 bar is 14.5 ˚C and 64.6 °C respectively, and varies slightly with the CO_2 pressure.

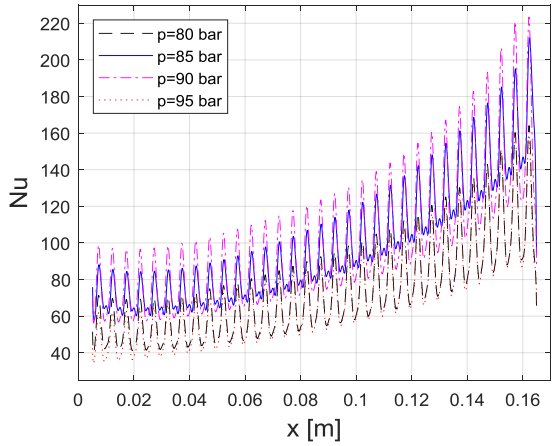

Figure 9: Variation of Nusselt number along the cold surface

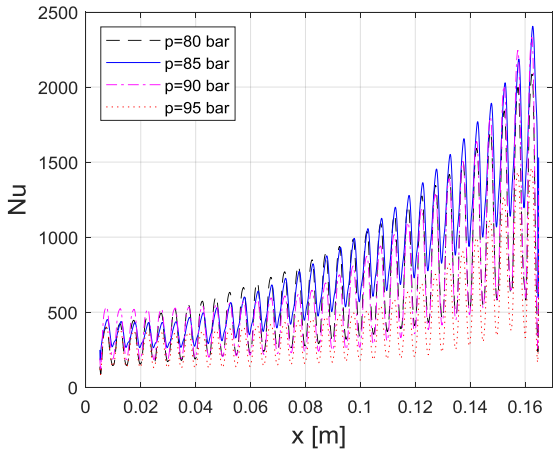

Figure 10: Variation of Nusselt number along the hot surface

Figure 11 shows the averaged Nusselt number along the middle plate for both hot and cold sides. For CO_2 side (hot), the average Nusselt number reaches its maximum value at 85 bar and then drops, suggesting it as an optimum pressure for enhancing the rate of heat transfer between the CO_2 and the HTF.

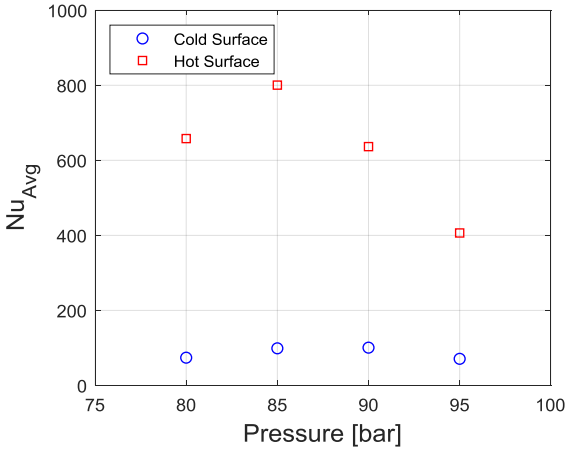

Figure 11: Variation of surface averaged Nusselt number along the cold and hot surfaces

5. CONCLUSIONS

In this work, a commercial 20 plate heat exchanger is numerically modeled as a simplified 2D corrugated plate with zero chevron angle. The simulated heat exchanger surface area is set to match the total surface area of the 20-plate heat exchanger. Among the real gas models tested in the simulation, the Redlich-Kwong model converges fastest with almost identical results like those obtained with the other models. An extra 50% surface area is added in the 2D simulation to reflect the chevron angle effect and match the numerical heat exchanger results to the experimental ones within 7%. The numerical results of the heat exchanger outlet temperatures exhibit a similar trend versus CO_2 working pressures like the experimental results. The simplified 2D numerical model could reduce computational costs compared to those associated with 3D PHE numerical studies.

NOMENCLATURE

c_p	Specific heat capacity, (J/(kg·K))
GC	Gas cooler
GWP	Global warming potential
HTF	Heat transfer fluid
k	Thermal conductivity, (W/(m·K))
Nu	Nusselt number, (-)
p	Pressure, (bar)
PHE	Plate heat exchanger
R	Molar gas constant, (J/(mol·K))
SSL	Stainless-steel
T	Temperature, (°C or K)
U	Velocity vector, (m/s)
V	Specific molar volume, (m^3/mol)
V_d	Compressor swept volume, (m^3)
y	Energy balance variable, (-)
$\dot{m}$	Mass flow rate, (kg/s)
$\dot{Q}$	Capacity rate, (W)
$\bar{u}$	Mean velocity, (m/s)
$\dot{W}$	Work per unit time (power), (W)
Greek symbols	
μ	Dynamic viscosity, (kg/(m·s))
ρ	Density, (kg/m^3)
δ	Kronecker delta, (-)
ν	Specific volume, (m^3/kg)
Subscript	
c	Critical
in	Inlet
out	Outlet

REFERENCES

ANSYS. (2016). ANSYS Fluent Theory Guide, Release 17.1.

Chakrabarti, Mitali, Montiel, A. P., Corrilo, I., He, J., Patti, A., . . . Schuermanns, K. (2017). CO2 Concentration in the Cabin in the Event of a Leak: CFD Simulation and Testing. *SAE Technical Paper*.

Galeazzo, F. C., Miura, R. Y., Gut, J. A., & Tadini, C. C. (2006). Experimental and numerical heat transfer in a plate heat exchanger. *Chemical Engineering Science, 61*, 7133-7138.

Han, W., Saleh, K., Aute, V., Ding, G., Hwang, Y., & Radermacher, R. (2011). Numerical simulation and optimization of single-phase turbulent flow in chevron-type plate heat exchanger with sinusoidal corrugations. *HVAC&R Research, 17*, 186-197.

Han, X.-H., Cui, L.-Q., Chen, S.-J., Chen, G.-M., & Wang, Q. (2010). A numerical and experimental study of chevron, corrugated-plate heat exchangers. *International Communications in Heat and Mass Transfer, 37*, 1008-1014.

Jain, S., Joshi, A., & Bansal, P. K. (2007). A new approach to numerical simulation of small sized plate heat exchangers with chevron plates.

Jalil, S. (2019). Phase-lags' Radial Variations Between Velocity, Shear Stress, and Pressure Gradient in Ultra-high Frequency Pulsating Turbulent Flows. *ASME J. Fluids Eng* .

Jalil, S. (2020). Numerical Characterization of Viscous Heat Dissipation Rate in Oscillatory Air Flow. *Journal of Heat Transfer, 142*(1), 011801.

Kauf, F. (1999). Determination of the optimum high pressure for transcritical CO2 refrigeration cycles. *International Journal of Thermal Sciences, 38*, 325-330.

Kim, M.-H., Pettersen, J., & Bullard, C. W. (2004). Fundamental process and system design issues in CO2 vapor compression systems. *Progress in energy and combustion science, 30*, 119-174.

Lemmon, E. W., Huber, M. L., & McLinden, M. O. (2013). NIST Standard Reference Database 23: Reference Fluid Thermodynamic and Transport Properties-REFPROP, Version 9.1, National Institute of Standards and Technology. doi:http://dx.doi.org/10.18434/T4JS3C

Liao, S. M., Zhao, T. S., & Jakobsen, A. (2000). A correlation of optimal heat rejection pressures in transcritical carbon dioxide cycles. *Applied Thermal Engineering, 20*, 831-841.

Lorentzen, G. (1994). Revival of carbon dioxide as a refrigerant. *International journal of refrigeration, 17*, 292-301.

Moffat, R. J. (1985). Using uncertainty analysis in the planning of an experiment. 173-178.

Müller, N., & Joseph, J. O. (2009). A Closer Look at CO2 as a Refrigerant. *ASHRAE Transactions, 115*.

Nekså, P. (2004). CO2 as Refrigerant for systems in transcritical operation. *Principles and Technology status, EcoLibrium, 3*, 26-31.

Okasha, A., & Müller, N. (2018). Simulation and Performance Correlation for Transcritical CO2 Heat Pump Cycle. *International Refrigeration and Air Conditioning Conference*, 2643.

Patankar, S. (1980). *Numerical heat transfer and fluid flow*. Hemisphere Publishing Corp.

Skočilas, J., & Palaziuk, I. (2015). CFD simulation of the heat transfer process in a chevron plate heat exchanger using the SST turbulence model.

Span, R., & Wagner, W. (1996). A new equation of state for carbon dioxide covering the fluid region from the triple-point temperature to 1100 K at pressures up to 800 MPa. *Journal of physical and chemical reference data, 25*, 1509-1596.

ACKNOWLEDGEMENT

Michigan State University thanks Ford Motor Company for its generous support of this research.